

Critical Delocalization of Chiral Zero Energy Modes in Graphene

Aires Ferreira^{1*}

¹*Department of Physics, University of York, York YO10 5DD, United Kingdom*

Eduardo R. Mucciolo²

²*Department of Physics, University of Central Florida, Orlando, Florida 32816, USA*

Graphene subjected to *chiral*-symmetric disorder is believed to host zero energy modes (ZEMs) resilient to localization, as suggested by the renormalization group analysis of the underlying nonlinear sigma model. We report accurate quantum transport calculations in honeycomb lattices with in excess of 10^9 sites and fine meV resolutions. The Kubo dc conductivity of ZEMs induced by vacancy defects (chiral BDI class) is found to match $4e^2/\pi h$ within 1% accuracy, over a parametrically wide window of energy level broadenings and vacancy concentrations. Our results disclose an unprecedentedly robust metallic regime in graphene, providing strong evidence that the early field-theoretical picture for the BDI class is valid well beyond its controlled weak-coupling regime.

PACS numbers: 72.80.Vp, 73.22.Pr, 73.23–b, 73.63.–b

After more than half a century, Anderson localization remains a central concept in condensed matter physics, with its many ramifications providing new insights into the behavior of disordered electrons [1]. The discovery of the “tenfold” symmetry classes of disordered metals [2, 3]—beyond the standard threefold Wigner-Dyson classification scheme—has revealed a surprisingly rich diagram of Anderson localization transitions, including multifractality and critical delocalization in low dimensions [4].

The interest in critical quantum transport in two-dimensional (2D) systems has been greatly amplified with the discovery of graphene, a one-atom-thick crystal endowed with massless Dirac fermions [5]. The internal pseudospin of the Dirac fermions—stemming from the honeycomb lattice structure with two sublattices—enables a rich variety of quantum transport phenomena [6, 7], including minimum conductivity in the clean limit [8], and crossover from weak-localization—orthogonal class—to weak-antilocalization—symplectic class—with increasing impurity potential range [9].

Recently, disordered graphene in the *chiral* symmetry class has been the focus of much attention [10–13]. In chiral models defined on bipartite lattices, disordered wave functions come in electron-hole pairs with energies $\pm E$ linked by a unitary matrix diagonal in the sublattice space, i.e., $|\phi_{\pm}\rangle = \hat{\sigma}_z |\phi_{\mp}\rangle$. A remarkable feature of the chiral class is the existence of *critical* states at the band center—zero-energy modes (ZEMs)—possessing multifractal statistics and absence of weak localization corrections at all orders in perturbation theory [2]. In graphene, the simplest realization of critical ZEMs is provided by randomly distributed vacancies. A vacancy is a topological defect obtained by cutting out all adjacent bonds to a given carbon site. Vacancies drastically affect the spectrum near the Dirac point, leading to the appearance of ZEMs with enhanced density of states (DOS) and quasilocated character [14, 15], which can be detected

by scanning tunneling microscopy [16]. Other examples of chiral-symmetric disorder in graphene include random non-Abelian gauge fields (ripples) [17], and resonant scatterers (e.g., adsorbed hydrogen) [18]. Whether quantum criticality induced by chiral disorder could explain the resilience of the minimum conductivity of graphene to Anderson localization is an outstanding question.

The focus of this Letter is on vacancy-induced ZEMs, recently implicated in a controversy regarding the exact nature of the quantum transport at the Dirac point [19–22]. Vacancy-defective graphene belongs to the chiral orthogonal ensemble (class BDI in the Altland-Zirnbauer classification of random fermion models [3]). The vanishing of the β -function of the effective nonlinear sigma model (NL σ M) led Ostrovsky *et al.* to conjecture a line of fixed points with nonuniversal metallic conductivity of the order of the conductance quantum $\sigma(0) \approx e^2/h$ [22–24]. However, the validity of the NL σ M of the BDI class has been questioned, as vacancies are infinitely strong scatterers, not amenable to perturbative analysis [12]. On the other hand, numerical evaluations of the conductivity using wave-packet propagation methods show localization of all states $\sigma(E) \rightarrow 0$, including the ZEMs [19–21]. The Gade singularity in the DOS approaching $E \rightarrow 0$ [12], however, raises questions on the validity of the extraction of the conductivity using wave-packet propagation methods.

In this Letter we report on accurate calculations of the longitudinal dc conductivity in macroscopic large disordered graphene. By employing an *exact* representation of the Kubo formula in terms of Chebyshev polynomials, we were able to extract the behavior of $\sigma(E)$ at the Dirac point with unprecedented resolution. Our results univocally show that vacancy-induced ZEMs display critical delocalization, as suggested by perturbative calculations based on the NL σ M [22–24] and numerical studies of the two-terminal conductance in nanoribbons with resonant scalar impurities [22, 23]. We find a *constant* conductiv-

ity over a wide range of vacancy concentrations,

$$\sigma(0) = \sigma_{\text{ZEM}} (1.00 \pm 0.01), \quad \sigma_{\text{ZEM}} \equiv \frac{4e^2}{\pi h}.$$

Strikingly, the ZEM conductivity is found to be robust with respect to variations in the inelastic broadening parameter η entering in the disordered Green functions down to $\eta = 2.5$ meV. This result is very surprising as vacancies are the ultimate case of a strong short-range disorder in graphene mixing K and K' valleys [6, 7].

The model.—Chiral disordered graphene is modeled by the standard tight-binding Hamiltonian of π electrons defined on a honeycomb lattice

$$\hat{H} = -t \sum_{\langle i,j \rangle} \left(\hat{a}_i^\dagger \hat{b}_j + \hat{b}_j^\dagger \hat{a}_i \right), \quad (1)$$

where $\langle i,j \rangle$ denotes nearest-neighbor pairs of carbon atoms and $t = 2.7$ eV is the corresponding hopping integral [5]. Periodic boundary conditions along zigzag and armchair directions are employed. The vacancies—obtained by removing the corresponding p_z orbitals—are distributed randomly on both sublattices with overall concentration n_i . In what follows, we briefly outline the Chebyshev-polynomial Green function method (CPGF) used to accurately evaluate spectral properties and response functions of real size systems.

The CPGF approach.—The numerical evaluation of the lattice resolvent operator $\hat{G}(z) = (z - \hat{H})^{-1}$ requires a nonzero broadening (*resolution*) parameter $\eta = \text{Im } z \gtrsim \delta E$, where δE is the mean level spacing. We are interested in the limit of small δE , where strong quantum interference effects associated with ZEMs can be fully appreciated [4]. Numerical evaluations of disordered lattice Green functions in the presence of critical states are computationally highly demanding. In Ref. [12] a time-domain stochastic method has been employed to extract the DOS with high resolution. Here, we evaluate target functions directly in the energy domain by expressing Green functions in terms of an *exact* polynomial expansion. Our approach turns out to be particularly advantageous in the calculation of the conductivity (see below). First-kind Chebyshev polynomials $\{T_n(x)\}_{n \in \mathbb{N}_0}$ are employed due to their superior convergence properties [25, 26]. The use of Chebyshev polynomials as a basis set requires rescaling the spectrum of \hat{H} into the interval $[-1 : 1]$. To this end, we scale both operators and energy variables, $\hat{H} \rightarrow \hat{h} = \hat{H}/W$, $\epsilon = E/W$, and $\lambda = \eta/W$, where W is the half-bandwidth. With this notation the Green function admits the following representation

$$\hat{G}(E + i\eta) = \frac{1}{W} \sum_{n=0}^{\infty} g_n(\epsilon, \lambda) \mathcal{T}_n(\hat{h}), \quad (2)$$

where $\{\mathcal{T}_n(\hat{h})\}$ are defined through the Chebyshev recursion relations: $\mathcal{T}_0(\hat{h}) = \hat{\mathbb{1}}$, $\mathcal{T}_1(\hat{h}) = \hat{h}$, and $\mathcal{T}_{n+1}(\hat{h}) =$

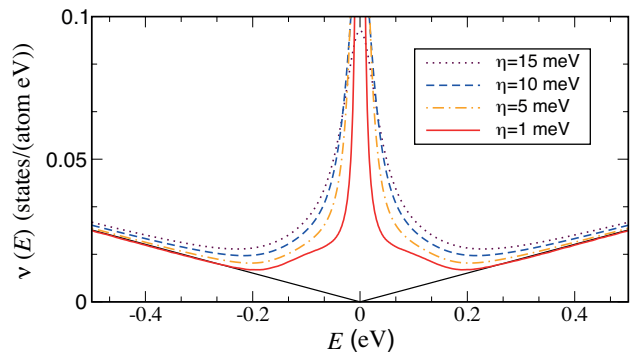


FIG. 1: Density of states of disordered graphene as function of Fermi energy. The Gade singularity of ZEMs is apparent as the energy levels are probed with increasing resolution $\eta \rightarrow 0$. The pristine DOS is shown (black line) as a guide to the eye.

$2\hat{h} \cdot \mathcal{T}_n(\hat{h}) - \mathcal{T}_{n-1}(\hat{h})$. The coefficients $\{g_n(\epsilon, \lambda)\}_{n \in \mathbb{N}_0}$ are system independent and possess a simple closed form [27]. The CPGF expansion (2) is the starting point of the accurate calculations reported in this work.

Density of states.—We start with a brief discussion of the DOS. Formally,

$$\nu(E) = -\frac{g_s}{\pi D} \text{Tr} \overline{\text{Im} \hat{G}(E + i\eta)}, \quad (3)$$

where $g_s = 2$ accounts for spin degeneracy and the bar means disorder averaging. According to Eqs. (2)–(3), the information about the DOS is contained in the Chebyshev moments $\nu_n = \text{Tr} \mathcal{T}_n(\hat{h})$ of individual disorder realizations. To probe features induced by chiral ZEMs with meV resolution, we consider a honeycomb lattice with $D = 60\,000 \times 60\,000$ sites ($\approx 94 \mu\text{m}^2$). This system has $\delta E \approx 0.3$ meV at the Dirac point in the absence of vacancies. The DOS for a dilute vacancy concentration $n_i = 0.4\%$ is shown in Fig. 1. Given the large size of the system simulated, one disorder configuration is sufficient to obtain very precise results. The expected enhancement of the DOS associated with ZEMs near $E = 0$ [14, 15] is seen to dramatically depend on the resolution. Extracting the exact scaling as $E \rightarrow 0$ is a demanding task as the number of Chebyshev moments required to converge the DOS, i.e., $N \propto W/\eta$, can be of the order of several tens of thousands even for meV resolution; here, $N = 15 \times 10^3$. (Similar technical challenges were encountered in Ref. [12].) The analysis of the data suggests that the singularity is stronger than that predicted by Gade and Wegner [2] in full consistency with the detailed numerical study of Ref. [12] and the analytical results in Ref. [13]; see Supplemental Material for full details [27].

Conductivity.—The finite-size Kubo formula reads

$$\sigma(E) = \frac{2\hbar e^2}{\pi \Omega} \text{Tr} \left[\overline{\text{Im} \hat{G}(E + i\eta) \hat{v}_{\parallel} \text{Im} \hat{G}(E + i\eta) \hat{v}_{\parallel}} \right], \quad (4)$$

where $\hat{v}_{\parallel} = [\hat{r}_{\parallel}, \hat{H}]/i\hbar$ is the velocity operator (taken along the zigzag direction) and Ω is the area. Here, the

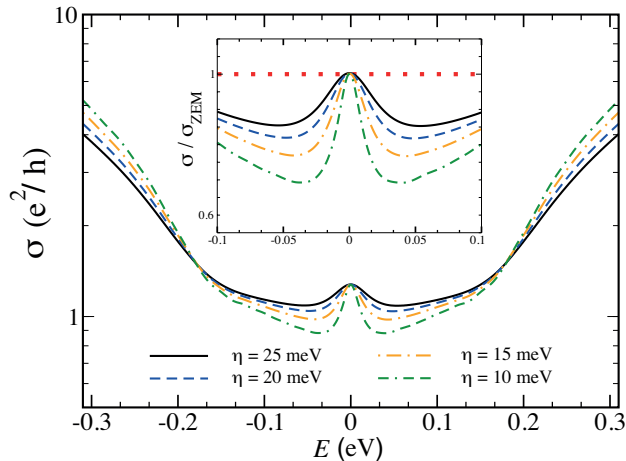


FIG. 2: Fully converged Kubo dc conductivity for a 0.4% vacancy concentration as a function of Fermi energy at selected values of η . The calculation required $N^2 = 6.4 \times 10^7$ Chebyshev moments. The inset shows a zoom of the peak at the Dirac point. Statistical fluctuations of the data are within $\approx 1\%$.

broadening η mimics the effect of uncorrelated inelastic scattering processes, thus defining a time scale $\tau_i = \hbar/\eta$ for phase coherence in the system [32, 33].

The calculation of $\sigma(E)$ follows identical steps as outlined for the DOS. The presence of two Green functions in Eq. (4) requires a double polynomial expansion, rendering the calculation computationally extremely demanding. Analogously to the kernel polynomial method [18, 25], the full spectral information is now contained in the Chebyshev moments $\sigma_{nm} = \text{Tr}[\mathcal{T}_n(\hat{h})\hat{v}_{\parallel}\mathcal{T}_m(\hat{h})\hat{v}_{\parallel}]$. The number of moments required ($\equiv N^2$) depends on the desired resolution. Typically, $N \approx 10 \times (W/\eta)$ converges the conductivity to two decimal places. From the knowledge of $\{\sigma_{nm}\}$ the dc conductivity $\sigma(E)$ is quickly reconstructed. See Ref. [27] for details.

Full spectral results.—We first provide a bird’s-eye view of $\sigma(E)$ before specializing to the case of ZEMs. For modest resolutions, $\eta \gtrsim 10$ meV, the physically meaningful limit $\sigma_{\Omega \rightarrow \infty}(E)$ is achievable in relatively small systems with $D \approx 10^7$. The fully converged dc conductivity for a dilute vacancy concentration $n_i = 0.4\%$ is shown in Fig. 2. The behavior of $\sigma_{\Omega \rightarrow \infty}(E)$ with decreasing η (i.e., increasing τ_i) provides direct information on the quantum transport regime [e.g., $\lim_{\eta \rightarrow 0} \sigma_{\Omega \rightarrow \infty}(E) = 0 (> 0)$ in the insulating (metallic) phase] [33]. The limit $\Omega \rightarrow \infty$ is implicit hereafter. In an energy window $\simeq \pm 0.2$ eV around $E = 0$ —excluding the Dirac point itself— $\sigma(E)$ decreases as η is lowered, showing that localization effects become increasingly more important as the thermodynamic limit $\eta \rightarrow \delta E \rightarrow 0$ is approached. The effect is notably stronger in the vicinity of the Dirac point, where strong localization ($\sigma \lesssim e^2/h$) takes place already

for $\eta \approx 10$ meV. This indicates that the *a priori unknown* simulated inelastic lengths $L_i = L_i(E, \tau_i)$ are sufficiently large that charge carriers can effectively experience localization. In contrast, at energies $|E| \gtrsim 0.2$ eV an increase of $\sigma(E)$ with increasing τ_i is observed. This suggests that at such energies the simulated L_i is not yet sufficiently large to observe localization effects. This interpretation is further confirmed below. At the Dirac point, on the other hand, $\sigma(E)$ seems insensitive to the inelastic broadening parameter, matching σ_{ZEM} with 1% precision in the entire range (see inset to Fig. 2). The anomalous robustness of the dc conductivity as $E \rightarrow 0$ is highly suggestive of a quantum critical point, in agreement with field-theoretical predictions [24].

High resolution results.—To probe the extension of delocalization effects at the Dirac point, we devise a scheme to enable the computation of $\sigma(E)$ with meV resolution. First, we recursively construct the vectors

$$|\varphi_{\pm}(E)\rangle = \frac{1}{W} \sum_{n=0}^{\infty} \text{Im}[g_n(\epsilon, \lambda)] \hat{\mathcal{O}}_{\pm}^n |\varphi\rangle, \quad (5)$$

where $|\varphi\rangle = \sum_{i=1}^D \chi_i |i\rangle$ is a real random vector, $\hat{\mathcal{O}}_{\pm}^n = \mathcal{T}_n(\hat{h})\hat{v}_{\parallel}$, and $\hat{\mathcal{O}}_{\pm}^n = \hat{v}_{\parallel}\mathcal{T}_n(\hat{h})$. The random variables $\{\chi_i\}$ are uncorrelated and taken from a uniform distribution with $\langle\langle\chi_i\rangle\rangle = 0$. The series is truncated at $n < N$ when convergence to the desired precision is achieved. Finally, the Kubo dc conductivity is obtained from

$$\sigma_{\varphi}(E) = \frac{2\hbar e^2}{\pi\Omega} \langle\varphi_{-}(E)|\varphi_{+}(E)\rangle, \quad (6)$$

by averaging with respect to both disorder and random vector realizations, i.e., $\sigma(E) = \langle\langle\sigma_{\varphi}(E)\rangle\rangle$ [27]. We note that for ZEMs, Eq. (5) acquires a particular simple form, $|\varphi_{\pm}(0)\rangle = W^{-1} \sum_n \text{Im}[g_{2n}(0, \lambda)] \hat{\mathcal{O}}_{\pm}^{2n} |\varphi\rangle$. The advantage of Eqs. (5) and (6) is that they do not require calculation of individual Chebyshev moments $\{\sigma_{nm}\}$ (cost $\propto N^2$). In practice, this allows us to reach fine resolution (higher N) and also much larger systems containing up to a few billion lattice sites [34].

The high-resolution conductivity data across the various transport regimes identified earlier is given in Fig. 3. For convenience, we define an *effective* system size $L_* \equiv \hbar\pi v_F/\eta$ as the length of a pristine graphene system having $\delta\epsilon = \eta$ at the Dirac point. The largest simulation has $L_* \simeq 0.7 \mu\text{m}$, corresponding to a broadening of only 2.5 meV. The state vectors in Eq. (5) were calculated with $N = 12000$ Chebyshev iterations. The ZEM conductivity shows no sign of localization, being numerically very close to $\sigma_{\text{ZEM}} = 4e^2/(\pi h)$ through a parametrically wide range of inelastic broadenings in the range [2.5, 60] meV. This is to be contrasted with the behavior of $\sigma(E)$ away from the band center. For instance, at energies $E = \{50, 100\}$ meV there is a strong suppression towards $\sigma \rightarrow 0$ as L_* increases. The localization is stronger in the neighborhood of the critical point at zero energy, with

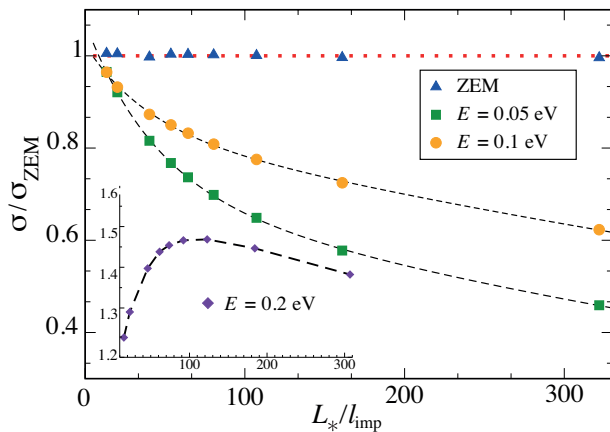


FIG. 3: Fully converged Kubo dc conductivity for a 0.4% vacancy concentration as a function of L_*/l_{imp} at selected energies. Here $l_{\text{imp}} \simeq 2.24$ nm is the average distance between vacancies. A large honeycomb lattice with 3.6×10^9 sites was simulated to obtain good precision at large L_* . Statistical fluctuations of the data are within $\simeq 1\%$.

states with $E = 50$ meV localizing first than those having $E = 100$ meV. This behavior can also be inferred from Fig. 2, which shows that the tendency as $\eta \rightarrow 0$ ($L_* \rightarrow \infty$) is for states to localize first in the vicinity of the ZEMs. In the inset to Fig. 3 the behavior for an energy far away from the Dirac point is shown. A transition from ballistic to localized regime is observed as L_* increases. Eventually, as $L_* \rightarrow \infty$, all states with $E \neq 0$ become localized. The latter is consistent with the behavior expected for random fermions in the BDI class [1, 4]. Crucially, however, our accurate numerical treatment shows that the chiral symmetry at $E = 0$ protects ZEMs from localization up to $L_* \approx 1 \mu\text{m}$. This exotic 2D metallic regime had been predicted by the renormalization group (RG) analysis of the NL σ M for the BDI class [24], although a fully nonperturbative calculation of the microscopic conductivity able to capture strong quantum interference effects at the Dirac point was lacking until now.

Universal ZEM conductivity.—We finally investigate the robustness of the ZEMs metallic conductivity against changes in vacancy concentration. According to the perturbative RG analysis for white-noise disorder in the BDI class, $\sigma(0)$ should depend weakly on the disorder strength [24]. The actual picture for vacancies—being infinitely strong scatterers—is difficult to predict based solely on field-theoretical methods [12, 35]. The little sensitivity of $\sigma(0)$ to the effective length L_* intuitively suggests a small dependence with the defect concentration too. Interestingly, numerical results for transport across narrow graphene strips show $\sigma(0) \approx \sigma_{\text{ZEM}}$ with weak dependence on n_i [23], demonstrating that, although evanescent modes are strongly affected by scattering from vacancy defects, the large number of modes available (large

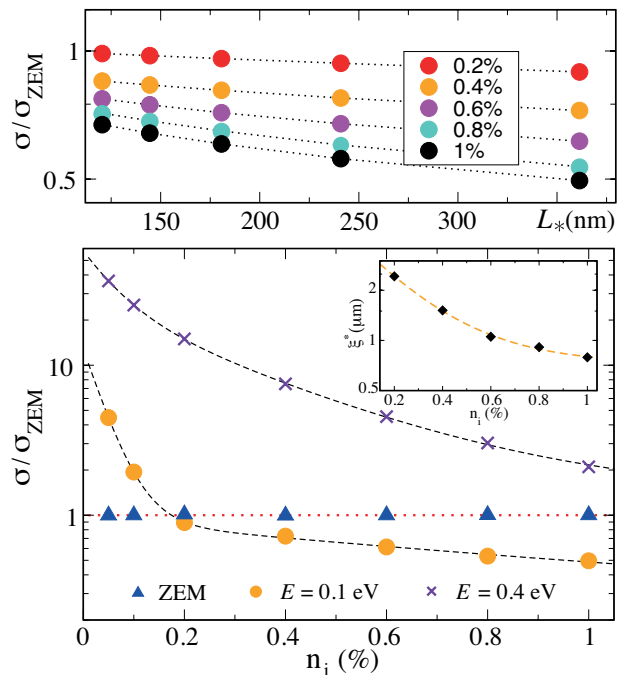


FIG. 4: Impact of vacancy concentration on bulk transport. Top panel: localization of states with $E = 0.1$ eV as a function of L_* at various vacancy concentrations. Bottom panel: variation of $\sigma(E)$ with n_i at selected energies.

DOS) counteracts perfectly to restore graphene’s clean ballistic conductivity [8]. To investigate the possibility of a disorder-induced universal metallic regime in graphene, we perform accurate Kubo calculations over 2 orders of magnitude in n_i . We take a fine broadening $\eta = 2.5$ meV so as to guarantee that L_* is sufficiently large to capture any marked localization trend near the Dirac point. Our results are summarized in Fig. 4. Away from the band centre the conductivity is strongly decaying with n_i as expected. For instance, at $E = 0.1$ eV—a typical Fermi energy in experiments—the conductivity swiftly enters in the strong localized regime already for dilute concentrations $n_i \approx 0.2\%$. The dependence of $\sigma(E)$ with L_* is well fitted by an exponential law $\sigma \propto e^{-L_*/\xi_*}$; see top panel. (The dependence of ξ_* with the defect concentration is shown in the inset to the bottom panel.) However, at the band centre ZEMs show no signs of localization even beyond the very dilute limit up to concentrations $n = 1\%$. For completeness we provide the results for $E = 0.4$ eV where transport is ballistic in the simulated range of L_* up to $n \approx 0.8\%$ (see also Fig. 3).

We briefly comment on previous wave-packet propagation calculations reporting on $\sigma(0) \rightarrow 0$ [19–21]. The strong singularity of the DOS at $E = 0$ makes the numerical extraction of the conductivity from the Einstein relation for diffusive transport $\sigma(E) \propto \nu(E)D(E)$ very challenging. Additionally, the level broadening inserted as the inverse of the time cutoff in the wave packet propa-

gation may not be equivalent to the broadening employed in the finite-size Kubo formula [Eq. (4)]. Although computationally much more demanding, our approach has the advantage of assessing directly the microscopic conductivity with no further assumptions.

In summary, we have demonstrated critical delocalization of zero energy modes in graphene by means of accurate numerical evaluations of the Kubo conductivity in real size disordered systems containing billions of carbon atoms. Rather remarkably, the absence of localization in the BDI class at the Dirac point is consistent with nonlinear sigma model predictions [24] and numerical studies of the Dirac equation [22, 23], suggesting an unprecedentedly robust metallic state in two dimensions. We hope that our work further encourages the use of accurate large-scale polynomial methods in the study of Anderson localization transitions.

A. F. acknowledges M. D. Costa for technical discussions and high-performance computing (HPC) support. The calculations were performed in HPC facilities based at the Graphene Research Centre, National University of Singapore. A. F. is thankful for the partial support from the National Research Foundation, Prime Minister Office, Singapore, under its Competitive Research Programme (Grant No. R-144-000-295-281). A. F. gratefully acknowledges the financial support of the Royal Society (U.K.) through a Royal Society University Research Fellowship.

* Electronic address: aires.ferreira@york.ac.uk

- [1] *50 Years of Anderson Localization*, edited by E. Abrahams (World Scientific, Singapore, 2010).
- [2] R. Gade and F. Wegner, Nucl. Phys. B **360**, 213 (1991); R. Gade, Nucl. Phys. B **398**, 499 (1993).
- [3] M. R. Zirnbauer, J. Math. Phys. **37**, 4986 (1996); A. Altland and M. R. Zirnbauer, Phys. Rev. B **55**, 1142 (1997).
- [4] F. Evers and A. D. Mirlin, Rev. Mod. Phys. **80**, 1355 (2008).
- [5] A. H. Castro Neto, F. Guinea, N. M. R. Peres, K. S. Novoselov, and A. K. Geim, Rev. Mod. Phys. **81**, 109 (2009).
- [6] N. M. R. Peres, Rev. Mod. Phys. **82**, 2673 (2010).
- [7] E. R. Mucciolo and C. H. Lewenkopf, J. Phys.: Condens. Matter **22**, 273201 (2010).
- [8] M. I. Katsnelson, Eur. Phys. J. B **51**, 157 (2006).
- [9] H. Suzuura and T. Ando, Phys. Rev. Lett. **89**, 266603 (2002).
- [10] L. Schweitzer and P. Markoš, Phys. Rev. B **85**, 195424 (2012).
- [11] G. Usaj, P. S. Cornaglia, and C. A. Balseiro, Phys. Rev. B **89**, 085405 (2014).
- [12] V. Hafner, J. Schindler, N. Weik, T. Mayer, S. Balakrishnan, R. Narayanan, S. Bera, and F. Evers, Phys. Rev. Lett. **113**, 186802 (2014).
- [13] P. M. Ostrovsky, I. V. Protopopov, E. J. Konig, I. V. Gornyi, A. D. Mirlin, and M. A. Skvortsov, Phys. Rev. Lett. **113**, 186803 (2014).
- [14] V. M. Pereira, F. Guinea, J. M. B. Lopes dos Santos, N. M. R. Peres, and A. H. Castro Neto, Phys. Rev. Lett. **96**, 036801 (2006).
- [15] V. M. Pereira, J. M. B. Lopes dos Santos, and A. H. Castro Neto, Phys. Rev. B **77**, 115109 (2008).
- [16] M. M. Ugeda, I. Brihuega, F. Guinea, and J. M. Gomez-Rodriguez, Phys. Rev. Lett. **104**, 096804 (2010).
- [17] D. Huertas-Hernando, F. Guinea, and A. Brataas, Phys. Rev. Lett. **103**, 146801 (2009).
- [18] A. Ferreira, J. Viana-Gomes, J. Nilsson, E. R. Mucciolo, N. M. R. Peres, and A. H. Castro Neto, Phys. Rev. B **83**, 165402 (2011).
- [19] Z. Fan, A. Uppstu, and A. Harju, Phys. Rev. B **89**, 245422 (2014).
- [20] G. Trambly de Laissardiere, and D. Mayou, Phys. Rev. Lett. **111**, 146601 (2013).
- [21] A. Cresti, F. Ortman, T. Louvet, D. Van Tuan, and S. Roche, Phys. Rev. Lett. **110**, 196601 (2013).
- [22] S. Gattenlohner, W.-R. Hannes, P. M. Ostrovsky, I. V. Gornyi, A. D. Mirlin, and M. Titov, Phys. Rev. Lett. **112**, 026802 (2014).
- [23] P. M. Ostrovsky, M. Titov, S. Bera, I. V. Gornyi, and A. D. Mirlin, Phys. Rev. Lett. **105**, 266803 (2010).
- [24] P. M. Ostrovsky, I. V. Gornyi, and A. D. Mirlin, Phys. Rev. B **74**, 235443 (2006).
- [25] A. Weisse, G. Wellein, A. Alvermann, and H. Fehske, Rev. Mod. Phys. **78**, 275 (2006).
- [26] J. P. Boyd, *Chebyshev and Fourier Spectral Methods*, 2nd edition (Dover Publications, 2001).
- [27] See Supplemental Material attached below (pages 6-12) for details on the Chebyshev-polynomial Green function (CPGF) method as well as a thorough description of the accurate large-scale numerical calculations presented in the Letter, which includes Refs. [28–31].
- [28] A. Ferreira (to be published).
- [29] H. Tal-Ezer and R. Kosloff, J. Chem. Phys. **81**, 3967 (1984).
- [30] I. S. Gradshteyn and I. M. Ryzhik. *Table of Integrals, Series, and Products*, 7th Edition (Elsevier, Academic Press, 2007).
- [31] T. Iitaka and T. Ebisuzaki, Phys. Rev. E **69**, 057701 (2004).
- [32] D. J. Thouless and S. Kirkpatrick, Phys. C: Solid State Phys. **14**, 235 (1981).
- [33] Y. Imry, *Introduction to mesoscopic physics*, 2nd edition (Oxford University Press, 2002).
- [34] A single realization of a system with $D = 3.6 \times 10^9$ atoms with N up to 12000 takes only a few days of HPC time if enough memory (typically 0.5 TB) is available to recursively construct the huge vectors $|\varphi_{\pm}(E)\rangle$ on the fly.
- [35] E. J. Konig, P. M. Ostrovsky, I. V. Protopopov, and A. D. Mirlin, Phys. Rev. B **85**, 195130 (2012).

Supplemental Material for “Critical delocalization of chiral zero energy modes in graphene”

We provide details on the Chebyshev-polynomial Green function (CPGF) method as well as a thorough description of the accurate large-scale numerical calculations presented in the main text.

I. CHEBYSHEV-POLYNOMIAL GREEN FUNCTION (CPGF) METHOD

At the heart of the CPGF method is the exact expansion of the Green function $\hat{\mathcal{G}}(z) = (z - \hat{h})^{-1}$ for a disordered lattice in terms of first-kind Chebyshev polynomials [1]. Below, we provide a short description of their main properties and a brief derivation of the CPGF expansion.

We assume that the spectrum of \hat{h} falls in the interval $\mathcal{I} = [-1 : 1]$ [2]. Accordingly, in what follows, z is a rescaled complex energy variable, $z := \epsilon + i\lambda$ with $\lambda > 0$. Chebyshev polynomials $\{T_n(x)\}_{n \in \mathbb{N}_0}$ satisfy the recursion relations

$$T_0(x) = 1, \quad T_1(x) = x, \quad T_{n+1}(x) = 2xT_n(x) - T_{n-1}(x), \quad (1)$$

such that $T_n(x) = \cos(n \arccos x)$. They obey the orthogonality relations

$$\int_{\mathcal{I}} dx \omega(x) T_n(x) T_m(x) = \frac{1 + \delta_{n,0}}{2} \delta_{n,m}, \quad (2)$$

where $\omega(x) = 1/(\pi\sqrt{1-x^2})$, thus forming a complete set in the domain \mathcal{I} . For a function $f(x)$ and $x \in \mathcal{I}$ one can write the expansion

$$f(x) = \omega(x) \sum_{n=0}^{\infty} \frac{2\mu_n}{1 + \delta_{n,0}} T_n(x), \quad (3)$$

where $\mu_n = \int_{\mathcal{I}} dx f(x) T_n(x)$. Upon truncation of the expansion, the Chebyshev polynomials distribute errors uniformly, providing a superior polynomial expansion with uniform resolution $\delta x \propto 1/N$, where N is the highest polynomial order used [3].

Let $\{\epsilon_m\}$ and $\{|m\rangle\}$ be the eigenvalues and eigenvectors of the Hamiltonian \hat{h} . In order to find an exact expansion of the lattice Green function,

$$\hat{\mathcal{G}}(\epsilon + i\lambda) = \sum_m \frac{|m\rangle\langle m|}{\epsilon + i\lambda - \epsilon_m}, \quad (4)$$

in terms of Chebyshev polynomials, we make use of the identity [4]

$$e^{-ixz} = \sum_{n=0}^{\infty} \frac{2i^{-n}}{1 + \delta_{n,0}} J_n(z) T_n(x), \quad |x| \leq 1, \quad (5)$$

where $J_n(z)$ is the Bessel function of order n , to recast (4) as

$$\hat{\mathcal{G}}(\epsilon + i\lambda) = \frac{1}{i} \int_0^{\infty} dt e^{i(\epsilon+i\lambda)t} \left[\sum_{n=0}^{\infty} \frac{2i^{-n}}{1 + \delta_{n,0}} J_n(t) \mathcal{T}_n(\hat{h}) \right], \quad (6)$$

where $\{\mathcal{T}_n(\hat{h})\}$ are operators defined by the matrix version of the Chebyshev recursion relations (1), that is,

$$\mathcal{T}_0(\hat{h}) = \mathbb{I}_D, \quad \mathcal{T}_1(\hat{h}) = \hat{h}, \quad \mathcal{T}_{n+1}(\hat{h}) = 2\hat{h} \cdot \mathcal{T}_n(\hat{h}) - \mathcal{T}_{n-1}(\hat{h}), \quad (7)$$

with D denoting the Hilbert space dimension. The Laplace transform of the Bessel function has a well-known solution [5]

$$\int_0^{\infty} dt e^{-st} J_n(t) = \frac{1}{\sqrt{1+s^2}} \left(\sqrt{1+s^2} - s \right)^n. \quad (8)$$

Using this expression, after the analytic continuation $s \rightarrow -iz$ and some straightforward algebra one obtains [1]

$$\hat{\mathcal{G}}(\epsilon + i\lambda) = \sum_{n=0}^{\infty} g_n(\epsilon + i\lambda) \mathcal{T}_n(\hat{h}), \quad (9)$$

$$g_n(z) \equiv \frac{2i^{-1}}{1 + \delta_{n,0}} \frac{(z - i\sqrt{1-z^2})^n}{\sqrt{1-z^2}}. \quad (10)$$

In what follows we show how to use the CPGF expansion (9) to compute spectral properties of large systems.

II. APPLICATION: DOS AND LONGITUDINAL DC CONDUCTIVITY

The thermodynamic density of states (DOS) is formally given by $\rho(\epsilon) = \lim_{\lambda \rightarrow 0} \lim_{D \rightarrow \infty} \nu(\epsilon, \lambda)$ where

$$\nu(\epsilon, \lambda) = -\frac{1}{\pi D} \text{Tr} \overline{\text{Im} \hat{\mathcal{G}}(\epsilon + i\lambda)}. \quad (11)$$

Here bar denotes disorder averaging. Using Eq. (9) we easily obtain

$$\nu(\epsilon, \lambda) = -\frac{1}{\pi D} \sum_{n=0}^{\infty} \text{Im}[g_n(\epsilon + i\lambda)] \mu_n, \quad (12)$$

with Chebyshev moments given by

$$\mu_n = \text{Tr}[\mathcal{T}_n(\hat{h})]. \quad (13)$$

Similarly to the kernel polynomial method (KPM) [6], the calculation of the DOS amounts to the determination of the Chebyshev moments. This scheme is very convenient as $\{\mu_n\}$ can be efficiently calculated even in very large systems with modest computational resources. Once the moments are determined, the smeared DOS in the entire parameter space (ϵ, λ) can be quickly retrieved from Eq. (12).

In a practical calculation the expansion is truncated so as to obtain an order- N approximation to the target function,

$$\nu_N(\epsilon, \lambda) = -\frac{1}{\pi D} \sum_{n=0}^{N-1} \text{Im} [g_n(\epsilon + i\lambda)] \mu_n. \quad (14)$$

For not too small λ , extremely accurate approximations can be obtained for modest N . However, the extraction of the thermodynamic limit almost invariably requires large N . The recursive calculation of Chebyshev moments $\{\mu_n\}$ explore the matrix relations in Eq. (7) and is numerically very stable. Furthermore, the Chebyshev expansion has well defined resolution [through the broadening parameter appearing in the Green function (4)]. These are two substantial advantages of polynomial methods as compared to, e.g., Lanczos recursion [6]. Notice that kernel coefficients are absent in Eq. (14); thus, this expansion is not equivalent to that obtained through the KPM [1].

The convergence rate of the exact expansion (14) depends crucially on the smoothness of the target function. As shown by the authors in Ref. [7] the presence of sharp resonances in the DOS requires a particularly large number of moments. As a rule of thumb, the number of Chebyshev moments N determine the resolution $\delta\epsilon_N$ according to $\delta\epsilon_N \approx 1/N$ [6]. For instance, to probe features with small width η an accurate calculation requires $\delta\epsilon_N \lesssim \eta$ and hence many Chebyshev moments before the expansion (14) converges [7, 28].

Next we discuss the application of the CPGF to the calculation of the dc conductivity. The starting point is the finite-size Kubo formula at zero temperature,

$$\sigma(\epsilon, \lambda) = \frac{2\hbar e^2}{\pi\Omega} \text{Tr} \left[\overline{\text{Im} \hat{\mathcal{G}}(\epsilon + i\lambda) \hat{v}_x \text{Im} \hat{\mathcal{G}}(\epsilon + i\lambda) \hat{v}_x} \right], \quad (15)$$

where $\hat{v}_x = [\hat{x}, \hat{h}]/i\hbar$ is the velocity operator and Ω is the area. Here, the broadening parameter λ defines a time scale $\tau_i \propto 1/\lambda$ for phase coherence in the system [8]. Using Eq. (9) we easily find

$$\sigma_N(\epsilon, \lambda) = \frac{2\hbar e^2}{\pi\Omega} \sum_{n,m=0}^{N-1} \text{Im}[g_n(\epsilon + i\lambda)] \text{Im}[g_m(\epsilon + i\lambda)] \mathcal{V}_{nm}, \quad (16)$$

where

$$\mathcal{V}_{nm} = \text{Tr} \left[\hat{v}_x \mathcal{T}_n(\hat{h}) \hat{v}_x \mathcal{T}_m(\hat{h}) \right]. \quad (17)$$

The evaluation of the dc conductivity is computationally more demanding than the DOS due to the presence of a double sum in Eq. (16). The number of moments is now N^2 , which can severely limit the resolutions and/or system size attainable. However, as shown in what follows, this limitation can be overcome if enough memory exists to store the random vectors used for a stochastic evaluation of the moments.

III. EFFICIENT CALCULATION OF CHEBYSHEV MOMENTS

The complexity of the trace evaluation in Eqs. (13) and (17) is $\mathcal{O}(D^2)$. However, for very large sparse matrices, such as those appearing in effective tight-binding models, the full trace can be replaced by a stochastic average. For instance, for the DOS one can replace Eq. (13) by

$$\mu_n \approx \frac{1}{R} \sum_{r=1}^R \langle r | \mathcal{T}_n(\hat{h}) | r \rangle, \quad (18)$$

where $|r\rangle = \sum_{i=1}^D \xi_i |i\rangle$ are complex random vectors with coefficients satisfying $\langle \xi_i \rangle = 0$ and $\langle \xi_i^* \xi_j \rangle = \delta_{ij}$ (real vectors may be used for spin rotational and time reversal symmetric Hamiltonians) [9]. The number of operations required to compute (18) is now $\mathcal{O}(D \times R)$.

It is often assumed that the error in (18) has the very favorable scaling $\mathcal{O}(1/\sqrt{RD})$ [6]. However, for very large n the matrix $\mathcal{T}_n(\hat{h})$ is no longer sparse and a larger R (or a larger system size D) is needed to obtain a stochastic trace evaluation (STE) with good precision. In practice, for very large systems, with $D \approx 10^9$, we found that a single random vector is enough to obtain errors below 1% for n up to ten thousand. Details are given below.

We now overview the recursive method that allows us to efficiently calculate Chebyshev moments. For a general introduction the reader is referred to the review by A. Weisse *et al.* [6]. For concreteness, we describe the calculation of conductivity moments, i.e.,

$$\mathcal{V}_{nm} = \frac{1}{R} \sum_{r=1}^R \langle r | \hat{v}_x \mathcal{T}_n(\hat{h}) \hat{v}_x \mathcal{T}_m(\hat{h}) | r \rangle. \quad (19)$$

(The DOS moments are computed with a similar scheme.) Suppose we start with a random vector $|r\rangle$. Then, using the recursion relations [Eq. (7)], we obtain

$$\mathcal{T}_{m+1}(\hat{h})|r\rangle = 2\hat{h} \mathcal{T}_m(\hat{h})|r\rangle - \mathcal{T}_{m-1}(\hat{h})|r\rangle, \quad (20)$$

which inspires us to write

$$|r\rangle_{m+1} = 2\hat{h}|r\rangle_m - |r\rangle_{m-1}, \quad (21)$$

where

$$|r\rangle_m = \mathcal{T}_m(\hat{h})|r\rangle. \quad (22)$$

In the above, $|r\rangle_0 = |r\rangle$. In fact, the best way to proceed is to define a second, auxiliary truncated basis $\{|\bar{r}\rangle\}$, $\bar{r} = 1, \dots, R$, with

$$|\bar{r}\rangle = \hat{v}_x |r\rangle. \quad (23)$$

Then, we can apply the Chebyshev recursion to write

$$|\bar{r}\rangle_{n+1} = 2\hat{h}|\bar{r}\rangle_n - |\bar{r}\rangle_{n-1}. \quad (24)$$

The idea now is to implement a recursive calculation for each pair of random vectors, $\{|r\rangle\}$ and $\{|\bar{r}\rangle\}$, to generate two sequences $\{|r\rangle_0, \dots, |r\rangle_{N-1}\}$ and $\{|\bar{r}\rangle_0, \dots, |\bar{r}\rangle_{N-1}\}$, since they can be used to directly compute the stochastic averages

$$\mathcal{V}_{nm}(r) = {}_n\langle \bar{r} | \hat{v}_x | r \rangle_m \quad (25)$$

needed for the calculation of the conductivity moments (19), i.e.,

$$\mathcal{V}_{nm} = \frac{1}{R} \sum_{r=1}^R \mathcal{V}_{nm}(r). \quad (26)$$

If large amounts of RAM are available, one can recursively compute $\{|r\rangle_n\}$ and $\{|\bar{r}\rangle_m\}$ for all $n, m = 0, \dots, N-1$, store them, and then evaluate the coefficients $\mathcal{V}_{nm}(r)$ for each r [no need to store $\{|r\rangle_n\}$ and $\{|\bar{r}\rangle_m\}$ for more than a given r at any time] [10].

We now show how to evaluate efficiently the matrix elements $\mathcal{V}_{nm}(r) = {}_n\langle \bar{r} | \hat{v}_x | r \rangle_m$ using a site representation for the random vector. Let

$$\psi_n^{(r)}(x_k, y_k) = \langle x_k, y_k | r \rangle_n, \quad \phi_m^{(r)}(x_k, y_k) = \langle x_k, y_k | \bar{r} \rangle_m, \quad (27)$$

with $k = 1, \dots, D$, where (x_k, y_k) are lattice site coordinates. Then,

$$\begin{aligned} \mathcal{V}_{nm}(r) &= \sum_{k, k'=1}^D [\phi_m^{(r)}(x_k, y_k)]^* \psi_n^{(r)}(x_{k'}, y_{k'}) \times \\ &\quad \times \langle x_k, y_k | \hat{v}_x | x_{k'}, y_{k'} \rangle. \end{aligned} \quad (28)$$

We can write

$$\langle x_k, y_k | \hat{v}_x | x_{k'}, y_{k'} \rangle = i(x_{k'} - x_k) \langle x_k, y_k | \hat{h} | x_{k'}, y_{k'} \rangle. \quad (29)$$

When only nearest-neighbor hopping is allowed, there is a substantial reduction in the number of terms required to compute the matrix element:

$$\begin{aligned} \mathcal{V}_{nm}(r) &= i \sum_{k=1}^D [\phi_m^{(r)}(x_k, y_k)]^* \sum_{\tau} \tau_x \psi_n(x_k + \tau_x, y_k + \tau_y) \times \\ &\quad \times \langle x_k, y_k | \hat{h} | x_k + \tau_x, y_k + \tau_y \rangle, \end{aligned} \quad (30)$$

where the number of lattice vectors τ depends on the topology of the problem. The number of computational steps is thus precisely $D \times z$, which is much lower than D^2 . In most cases of interest, the Hamiltonian matrix element is just a constant hopping amplitude $-t_s$, in which case we have

$$\mathcal{V}_{nm}(r) = -i t_s \sum_{k=1}^D [\phi_m^{(r)}(x_k, y_k)]^* \sum_{\tau} \tau_x \psi_n(x_k + \tau_x, y_k + \tau_y). \quad (31)$$

Notice that t_s is a dimensionless hopping amplitude since, by construction, $|\pm \hat{h}| \leq 1$ (for graphene with vacancy

defects, $t_s \equiv t/W$ where t is the carbon-carbon hopping integral and W is half-bandwidth). Clearly, there is no need to store the entire $D \times D$ Hamiltonian matrix; a connectivity table with information about neighbor coordinates $\{n_1(x_k, y_k), \dots, n_z(x_k, y_k)\}_k$ suffices. This shows that the current scheme is just limited by the memory required to store the amplitudes $\{\psi_n^{(r)}\}_n, \{\phi_m^{(r)}\}_m$ needed to compute the overlap $\mathcal{V}_{nm}(r)$ for any two vectors $\{|r\rangle_n, |\bar{r}\rangle_m\}$.

The calculation can be made substantially more efficient if we are just interested in evaluating the conductivity in a small rectangular parametric grid $\{\{\epsilon_p\} \times \{\lambda_q\}\}$, $1 \leq p, q \leq p_{\max}, q_{\max}$. The Chebyshev moments \mathcal{V}_{nm} contain more information than any such grid since they allow one to retrieve the complete spectral conductivity according to Eq. (16). Recall that λ is only limited by the number of Chebyshev iterations, $\min \lambda \propto N^{-1}$, and hence can be made arbitrary small by increasing N . The conductivity for each point in the grid can be calculated efficiently using the *single-energy algorithm* outlined in the main text. The idea is to write the conductivity $\sigma_N(\epsilon_p, \lambda_q)$ for each pair $\{\epsilon_p, \lambda_q\}$ [see Eq. (16)] as

$$\sigma_N(\epsilon_p, \lambda_q) = \frac{2\hbar e^2}{\pi \Omega R} \sum_{r=1}^R \langle \varphi_-^{(r)}(\epsilon_p, \lambda_q) | \varphi_+^{(r)}(\epsilon_p, \lambda_q) \rangle, \quad (32)$$

where

$$|\varphi_+^{(r)}(\epsilon_p, \lambda_q)\rangle = \sum_{n=0}^{N-1} \text{Im}[g_n(\epsilon_p + i\lambda_q)] \hat{v}_x | r_n \rangle \quad (33)$$

and

$$|\varphi_-^{(r)}(\epsilon_p, \lambda_q)\rangle = \sum_{n=0}^{N-1} \text{Im}[g_n(\epsilon_p + i\lambda_q)] |\bar{r}_n\rangle. \quad (34)$$

Equations (33)-(34) can now be computed iteratively with only a few vectors stored in memory (instead of $2 \times N$ vectors). The substantial reduction in memory allocation has allowed us to treat very large tight-binding systems, in excess of a billion atoms ($D = 3.6 \times 10^9$), with high resolution; see next section.

IV. PARTICULAR CASE: GRAPHENE WITH RANDOM VACANCIES

In this section we provide the full numerical details of the calculations presented in the main text.

A. The DOS

The DOS of a macroscopic large honeycomb lattice ($N_x = N_y = 60000$; periodic boundary conditions) with dilute randomly distributed vacancies (concentration $n_i = 0.4\%$) has been calculated using the CPGF

method and numerical implementations as described above. The N -order approximation to the DOS is given by

$$\nu_N(E, \eta) = -\frac{1}{R} \sum_{n=0}^{N-1} \sum_{r=1}^R \frac{\text{Im}[g_n(\epsilon + i\lambda)]}{\pi DW} \langle r_n | r_n \rangle, \quad (35)$$

where $W = 3t$ is graphene's half-bandwidth and $|r_n\rangle$ as defined in Eq. (22), $E = \epsilon W$, and $\eta = \lambda W$. The initial random vector used in the Chebyshev recursion reads as $|r_0\rangle = \sum_{i=1}^D x_i |i\rangle$, where $\{x_i\}$ are generated from a uniform distribution on the interval $[-\sqrt{3}, \sqrt{3}]$. In such

a large Hilbert space ($D = N_x \times N_y = 3.6 \times 10^9$), self averaging guarantees that a single random vector $R = 1$ and one disorder realization suffice to obtain accurate results even for fine resolutions, that is, large N .

The accuracy of the stochastic evaluation of $\nu_N(\epsilon, \lambda)$ is illustrated with a few examples in Table I. The superior precision [better than 0.1% for zero-energy modes (ZEMs) investigated in the main text] is a consequence of the size of the system simulated. We note that at larger values of the resolution parameter λ (η) the data precision improves because convergence is achieved at smaller values of N (see below).

	ZEM	$E = 0.05$ eV	$E = 0.10$ eV	$E = 0.20$ eV
S_1	1.0782	2.1507×10^{-2}	1.6777×10^{-1}	1.11326×10^{-2}
S_2	1.0786	2.1495×10^{-2}	1.6764×10^{-1}	1.11259×10^{-2}
S_3	1.0784	2.1501×10^{-2}	1.6705×10^{-1}	1.11310×10^{-2}
$\max s_i \nu_{S_i} - \bar{\nu} /\bar{\nu}$	$\approx 0.02\%$	$\approx 0.03\%$	$\approx 0.30\%$	$\approx 0.35\%$

TABLE I: Estimation of the data precision. DOS [#states/(atom-eV)] for three independent system realizations (disorder and initial random vector $|r\rangle$), labeled S_1 , S_2 , and S_3 , at several energies for a resolution $\eta \equiv \lambda W$ of 1 meV. The relative maximum deviation from the average $\bar{\nu}$ is shown in the last row. The estimated accuracy is confirmed below using a different approach.

We now assess the convergence of the N -order approximation. N must be sufficiently large such that $\nu_N(\epsilon, \lambda)$ is well converged (say to 1% accuracy or better) for the smallest desired resolution λ . In Fig. 1, we show the variation of the DOS of ZEMs $\nu_N(0, \lambda)$ with N [see Eq. (35)]. The calculations highlight the need for many thousands of Chebyshev iterations when the spectrum is probed with fine resolutions (i.e., a few meV). Similar conclusions hold for other energies (not shown). For comparison we show the KPM approximation to the DOS using a Lorentz kernel [7, 25]. Despite being accurate in the limit $N \rightarrow \infty$, the KPM convergence rate is manifestly poorer in this case.

Having established the convergence and accuracy of the CPGF method in the case of graphene with vacancies, we show the fully converged DOS for 1 meV resolution in Fig. 2. A single system realization and random vector was employed. As an independent error estimator we use the electron-hole asymmetry degree, i.e., $|\nu_\infty(\epsilon, \lambda) - \nu_\infty(-\epsilon, \lambda)|/\nu_\infty(\epsilon, \lambda)$. The magnitude of the error and its dependencies with the Fermi energy are consistent with the earlier statistical analysis.

In order to illustrate the divergent behavior of the DOS at $E = 0$ we show in the right inset (Fig. 2) a plot of $E\nu(E, \eta)$ at several values of the resolution. According to the standard nonlinear sigma model picture [11], the thermodynamic DOS behaves as $\nu(E, 0) \rightarrow |E|^{-1} \exp[-|\ln |E||^{-1/2}]$ as $|E| \rightarrow 0$, whereas Häfner and

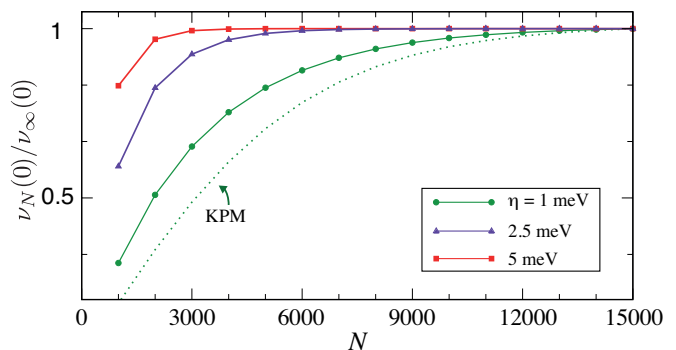


FIG. 1: Convergence of the N -order approximation to the DOS of ZEMs at selected values of resolution (broadening) parameter $\eta \equiv \lambda W$ with $W = 8.1$ eV. A single realization of a disordered system with $N_x = N_y = 60000$ and 0.4% vacancy concentration has been considered. The limiting value $\nu_{N \rightarrow \infty}(\epsilon, \lambda)$ has been estimated—with precision better than 1%—from the value of $\nu_N(\epsilon, \lambda)$ at $N = 15000$. The KPM result is shown (dotted line) for comparison.

co-workers observed a stronger singularity $\nu(E, 0) \rightarrow |E|^{-1} \ln |E|^{-x}$ with $2 > x \geq 1$ [12] in consistency with a recent prediction [13]. Our results indicate $E\nu(E, \eta) \rightarrow 0$ for η down to 1 meV, which is consistent with the numerical analysis of Ref. [12]. A more detailed analysis would be needed to reveal the exact dependence as obtained in the CPGF.

Our results show that the accurate determination of the spectral properties of disordered graphene is highly demanding, especially near the Gade singularity where fine resolutions are needed to capture the correct behavior. Similar challenges were reported in Ref. [12] where a time-domain stochastic method was used to extract the DOS. Finally, we note that the calculations are not sensitive to the system dimension as long as the mean level spacing is the smallest energy scale $\delta\epsilon \lesssim \lambda$. This makes the CPGF a convenient tool to extract the thermodynamic limit. In what follows, we show how the CPGF behaves for the calculation of the Kubo formula.

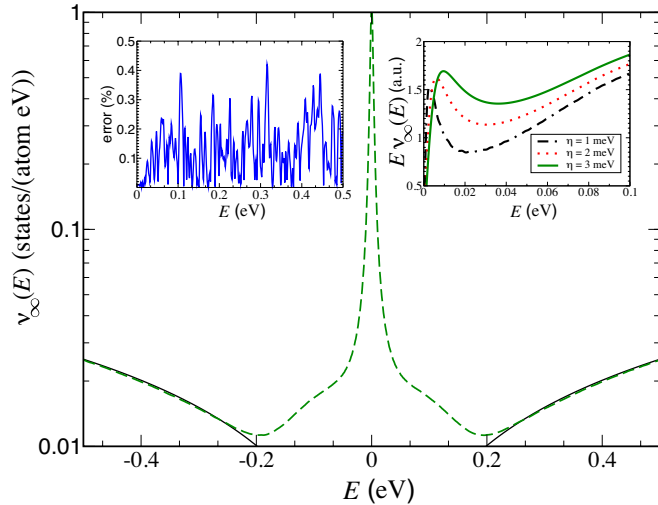


FIG. 2: DOS of graphene with vacancy defects ($n_i = 0.4\%$) as function of Fermi energy (green dashed line). The resolution of the calculation is $\eta = 1$ meV. A logarithmic scale has been chosen to highlight the singular behavior of $\nu(\epsilon, \lambda)$ as $\epsilon \rightarrow 0$. The solid black line shows the DOS of pristine graphene as a guide to the eye. The insets show the estimated error as function of Fermi energy (left) and a close look at the DOS singularity at $E = 0$ (right). The energy grid contains 1000 points.

B. dc conductivity

Below we provide the numerical details of the transport calculations presented in the main text. In Sec. B1 we focus on the full-spectrum algorithm used to produce the σ versus E curve in Fig. 2 (main text). Details of the high-resolution calculations with $D = 3.6 \times 10^9$ and N up to 12000 [Figs. 3 and 4 (main text)] are given in Sec. B2.

1. Full spectral results

As discussed in Sec. II, the knowledge of individual Chebyshev moments $\mathcal{V}_{nm} = \text{Tr} [\hat{v}_x \mathcal{T}_n(\hat{h}) \hat{v}_x \mathcal{T}_m(\hat{h})]$ enables the full spectral determination of the dc conductivity. However, an efficient numerical implementation

requires enough memory to store $2 \times N$ vectors of dimension D [see Eqs. (25)-(25)], which in practice limits the attainable D and/or N . To boost the size of the simulations we implemented the Chebyshev recursive method (Sec. III) in machines with large RAM. Having the sequences $\{|r\rangle_0, \dots, |r\rangle_{N-1}\}$ and $\{|\bar{r}\rangle_0, \dots, |\bar{r}\rangle_{N-1}\}$ stored in RAM allows for a quick evaluation of the Chebyshev moments through optimized linear algebra subroutines.

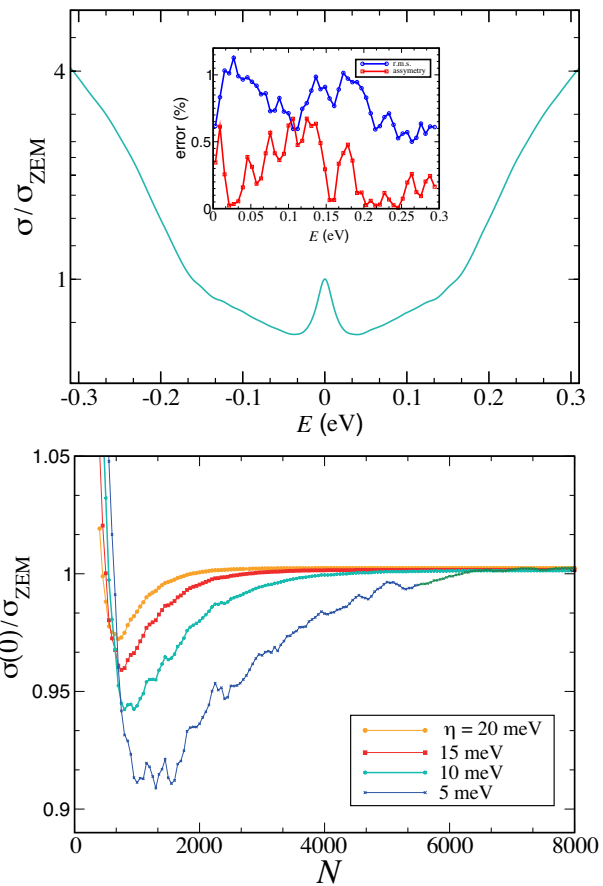


FIG. 3: Analysis of full-spectral results. **Top panel.** Conductivity of graphene with vacancy defects ($n_i = 0.4\%$) as function of Fermi energy. The resolution of the calculation is $\eta = 10$ meV [σ is given in units $\sigma_{\text{ZEM}} \equiv 4e^2/(\pi h)$]. The energy grids contain 1000 points. The inset shows the estimated error based on the standard deviation of 20 independent sets (each containing an average over 250 random vectors). For comparison, the error estimated using the electron-hole asymmetry degree is also shown. For clarity the grid in the inset contains only 49 points with $E > 0$. **Bottom Panel.** The convergence of the N -order approximation to the ZEMs microscopic conductivity $\sigma_N(0, \eta)$ is shown at selected values of η . Clearly, several thousands Chebyshev iterations (corresponding to tens of millions expansion moments \mathcal{V}_{nm}) are required as η enters the meV range.

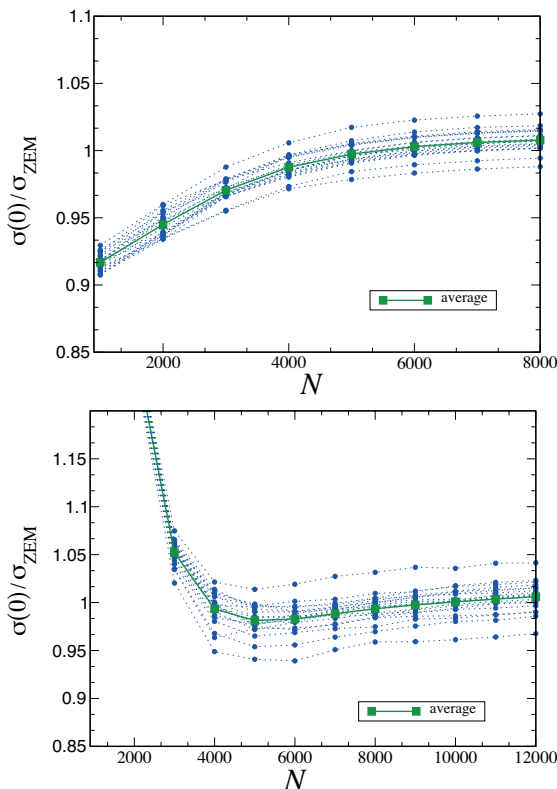


FIG. 4: Numerical analysis of the large-scale calculations. **Top panel.** “Single-shot” ZEM conductivity of realistic size graphene samples with a dilute concentration of vacancies ($n_i = 0.05\%$) as function of N . The resolution of the calculation is $\eta = 5$ meV. Each data set (blue circles) corresponds to a single system realization. The average over 20 independent system realizations is shown in squares. **Bottom Panel.** The same as in the left panel for $N = 12000$ polynomials and a resolution $\eta = 2.5$ meV.

The results reported in this section are for a honeycomb lattice with $D = 3200 \times 3200$ sites and a vacancy concentration $n_i = 0.4\%$. In order to extract the Kubo conductivity with satisfactory resolution we computed $N = 8000$ Chebyshev iterations [corresponding to $N^2 = 6.4 \times 10^7$ moments in the expansion of $\sigma_N(E, \eta)$, Eq. (16)]. The resulting $N \times N$ matrix is subsequently used to evaluate $\sigma_N(E, \eta)$ on a fine grid. D is large enough so that the thermodynamic limit $\Omega \rightarrow \infty$ can be safely extrapolated. In Fig. 3 (a) we show $\sigma(E) \equiv \lim_{\Omega \rightarrow \infty} \sigma_{N \rightarrow \infty}(E, \eta = 10 \text{ meV})$ for a fixed disorder realization. Here, E is the Fermi energy in eV.

Remarkably, the stochastic trace in Eq. (19) required thousands random vectors to converge $\sigma_N(E, \eta)$ to a good precision [14]. The high degree of electron-hole symmetry $\sigma(E, \eta) = \sigma(-E, \eta)$ achieved [see Fig. 3 (a)] testifies to the high quality of the results. The error in $\sigma_N(E, \lambda)$ is estimated to be in the range 0.1–1%. This is further confirmed with a detailed numerical study summarized in the inset to Fig. 3 (see caption for details).

The convergence of the N -order approximation for

ZEMs is shown in Fig. 3 (b). Whereas for poor resolutions ≈ 20 meV a few thousand Chebyshev iterations are sufficient, probing resolutions ≈ 1 meV is manifestly more demanding. Moreover, statistical fluctuations in the STE become important at small η , which requires more random vector realizations (see the noise in the curve for $\eta = 5$ meV). Importantly, all the curves studied converge to σ_{ZEM} to 1% accuracy, the main result of the Letter. A dedicated calculation at $E = 0$ will confirm this (see below).

2. Single-energy high-resolution results

In Sec. III we devised a “single-energy algorithm” that bypasses the computation of Chebyshev moments \mathcal{V}_{nm} , allowing us to reach much larger system sizes. We now describe its application to the problem of the ZEMs in graphene. The calculations summarized in this section are for a honeycomb lattice with $D = 3.6 \times 10^9$ sites. The huge system dimension results in $\sigma(E, \eta)$ data with satisfactory accuracy even for a single system realization, i.e., one random vector $R = 1$ and a single (vacancy) disorder realization. This situation is computationally very convenient as it provides a quick “single-shot” evaluation of the dc conductivity.

In Fig. 4 we show the variation of $\sigma_N(0, \eta)$ with N . As mentioned, a single system realization converges $\sigma_N(0, \eta)$ to a very reasonable precision (note that the vertical axis is zoomed around $\sigma = \sigma_{ZEM}$). The error bars increase slowly with N as the matrices $\mathcal{T}_n(\hat{h})$ become less and less sparse as $n \rightarrow N - 1$ for $N \gg 1$. For a dilute vacancy concentration $n_i = 0.05\%$ and broadening $\eta = 5$ meV, we obtain $\langle \overline{\sigma_{N=8000}(0)} \rangle = 1.008$ (in units of σ_{ZEM}) with standard deviation $\delta\sigma = 0.009$ (corresponding to 0.8% of the mean value). For the high resolution calculations ($\eta = 2.5$ meV), these values are $\langle \overline{\sigma_{N=12000}(0)} \rangle = 1.006$ and 0.016, respectively.

In the main text, a set of “single-shot” calculations with $\eta = \{2.5, 5, 7.5, 10, 12.5, 15, 20, 40, 60\}$ meV and $n_i = 0.4\%$ (Fig. 3), and $\eta = 5$ meV and $n_i = \{0.05, 0.1, 0.2, 0.4, 0.6, 0.8, 1\}\%$ (Fig. 4) were presented. In order to obtain a conservative estimate of the error bars involved we performed 20 independent realizations of the more disordered system, i.e., $n_i = 1\%$. We obtained $\langle \overline{\sigma_{N=8000}(0)} \rangle = 1.014$ with standard deviation 0.007, which suggests an accuracy of $\approx 1\%$.

Probing resolutions approaching 1 meV becomes increasingly more challenging as the number of iterations N increases considerably, and hence the number of random vectors necessary to converge the STE. We performed a small set of simulations for $\eta = 1$ meV ($N = 12000$, averaged over 2 disorder realizations and 10 random vectors) and obtained an average $0.95\sigma_{ZEM}$ with 5% standard deviation.

References

-
- * Electronic address: aires.ferreira@york.ac.uk
- [1] A. Ferreira, unpublished (2015).
- [2] Without loss of generality we have assumed a bound spectrum with $|\epsilon_m| \leq 1$. The latter can always be achieved by rescaling $\hat{H} \rightarrow \hat{h} = (\hat{H} - a_+ \mathbb{I})/a_-$ where $a_{\pm} = \frac{1}{2}(\max E_m \pm \min E_m)$.
- [3] J. P. Boyd, *Chebyshev and Fourier Spectral Methods*, second revised edition (Dover Publications, 2001).
- [4] H. Tal-Ezer and R. Kosloff, *J. Chem. Phys.* **81**, 3967 (1984).
- [5] I. S. Gradshteyn and I. M. Ryzhik. *Table of Integrals, Series, and Products*, 7th Edition (Elsevier, Academic Press, 2007).
- [6] A. Weisse, G. Wellein, A. Alvermann, and H. Fehske, *Rev. Mod. Phys.* **78**, 275 (2006).
- [7] A. Ferreira, J. Viana-Gomes, J. Nilsson, E. R. Mucciolo, N. M. R. Peres, and A. H. Castro Neto, *Phys. Rev. B* **83** 165402 (2011).
- [8] Y. Imry, *Introduction to mesoscopic physics*, 2nd edition (Oxford University Press, 2002).
- [9] T. Iitaka and T. Ebisuzaki, *Phys. Rev. E* **69**, 057701 (2004).
- [10] For a graphene system with 10 million atoms $D = 10^7$, and $N = 8 \times 10^3$ recursive steps, one needs ≈ 0.5 TB of RAM just to store all these vectors since a double precision number takes 8 bytes.
- [11] R. Gade and F. Wegner, *Nucl. Phys. B* **360**, 213 (1991); R. Gade, *Nucl. Phys. B* **398**, 499 (1993).
- [12] V. Häfner, J. Schindler, N. Weik, T. Mayer, S. Balakrishnan, R. Narayanan, S. Bera, and F. Evers, *Phys. Rev. Lett.* **113**, 186802 (2014).
- [13] P. M. Ostrovsky, I. V. Protopopov, E. J. König, I. V. Gornyi, A. D. Mirlin, and M. A. Skvortsov, *Phys. Rev. Lett.* **113**, 186803 (2014).
- [14] Usually it is assumed that the fluctuations in the stochastic trace evaluation are of the order of $1/\sqrt{RD}$, such that for large D a few random vectors are required [25, 31]. This result follows from the sparseness of the operators involved. However, in general the quality of the stochastic trace is very sensitive to the number of Chebyshev iterations. This happens because for large n (typically $n \approx \sqrt{D}$) the Chebyshev operator $T_n(\hat{h})$ is no longer sparse. To the best of our knowledge, this fact has remained unnoticed in previous works.